Journal of Fluids and Structures 17 (2003) 317–330

JOURNAL OF FLUIDS AND STRUCTURES

www.elsevier.nl/locate/jnlabr/yjfls

Multisolitons on vortex filaments: the origin of axial tangling

A. Maksimović, S. Lugomer*, I. Michieli

Department of Physics, Rudjer Bošković Institute, P.O. Box 1016, Bijenička c. 54, 10001 Zagreb, Croatia

Received 31 January 2001; accepted 9 August 2002

Abstract

The results of experimental and theoretical study of two-dimensional vortex filament tangling, appearing in laser–matter interactions on nanosecond time scale, are presented. A set of parallel vortex filaments shows various kinds of axial tangling as a consequence of excitation of multisolitons on filaments. It was shown that few basic types of the soliton combinations, either of (+) or (−) wave vector, or both, give rise of tangling of various degrees of topological complexity. Some of the "basic elements" of the filament organization, which repeat in the tangled structure, were obtained analytically by the Hirota method. The hierarchy in topological complexity of axial tangling of filaments originates from random shock waves (which generate solitons with alternating polarity), while random distribution of the multisoliton velocities causes various cases of their collision and spatial organization.

1. Introduction

Generation of vortex filaments and the onset of their tangling is a very intriguing physical process, and important for understanding of behavior (and of properties) of the so-called "vortex matter" (Crabtree and Nelson, 1997) in many systems like fluids, superfluids (Schwartz, 1998, 1985) in magnetic (geomagnetic) fluids (Jeanloz and Romanowicz, 1997), superconductors (Schönenberger et al., 1996; Kolton and Dominguez, 1999), as well as in astrophysical systems (Ricca and Berger, 1996; Geller and Huchra, 1989; Norman, 1996. It was demonstrated that vortex filaments can be formed also in laser–matter interaction (LMI) on short time scale (Lugomer and Maksimović, 1997; Lugomer, 1999). We assume that liquid metal generated in LMI at time scale $\tau = 10$ ns, behaves as ideal fluid during the first half of the laser pulse. In this time interval, the nonlinear and nonequilibrium processes take place, the result of which may be various kinds of self-organization (SO), among them, the formation of vortex filaments. Their spontaneous formation and their self-organization by various types of braiding was described by Lugomer (1999). The dissipative effects are, therefore, neglected in this period of the laser pulse. First, the maximum of the pulse intensity occurred, the temperature falls down and the viscosity increases in the second half of the pulse. The SO structures of vortex filaments formed in LMI with metal targets, in the first half of the laser pulse, stay frozen after pulse termination because of ultrafast cooling, thus enabling a posteriori analysis. Then, the dissipation, which sets in, occurs through vortex filament core spreading, through the change of their cross section from circular into elliptic one, and through their interaction with the background fluid. It was observed that braids of various complexity levels formed inside the laser spot give rise to filament tangling which is dominantly of the axial type. However, local transition to random tangling was also observed.

The tangling process occurs by: (i) the braiding of close filament bundles separated by distance $\sim\sigma$ (filament core size) (Lugomer, 1999), by reconnection of close filaments and (ii) by generation of various types of solitons (loops,

*Corresponding author. Fax: +385-1-4680-112.
E-mail address: lugomer@rudjer.irb.hr (S. Lugomer).

0889-9746/03/$ - see front matter
PII: S0889-9746(02)00120-2

kinks—left and right, etc.) on distant filaments (separated by distance $\gg\sigma$)—where braiding process is excluded. This paper presents the results of experimental and theoretical studies of the transition of vortex filaments into axially tangled structures (the filaments keep their parallelism), by the generation of various types of solitons (loops and kinks) with random velocity distribution.

2. Experimental results

Axial (and locally random) tangling of vortex filaments was generated by XeCl excimer laser ($\lambda = 308$ nm; $\tau = 16$ ns) on Cr-coated steel surface after $N = 13$ pulses. The experimental details are given in Lugomer (1999). Tangling of vortex filaments in LMI is caused by the shock waves traversing the sample in various directions because of reflection from the sample walls (the sample is small $\sim 1 \times 1$ cm so that fast shock waves return in the interaction space without significant damping). It is also caused by the oscillations (or by turbulence) of the background fluid in which the filaments (as separate entities) are immersed. Perturbation of filaments starts by their bending (in various directions) as well as by formation of loops. In some cases only a few loops, while in others a large series of loops is seen. They travel along the filament by simple sliding. In addition, there are filaments showing left and right kinks, of very complex type of tangling (the labyrinth type). In some cases, the kinks are small so that the filament does not touch the neighbor filament; in other cases the kinks are large, and the filament touch its distant neighbor what leads to their reconnection.

The three representative groups of the filament SO in LMI with different characteristics (geometrical and topological) are shown in Fig. 1A–C. Considering the SO of filaments in these micrographs, one can see that some "basic elements" of organization repeat along the filament(s). Such basic elements are the series of loops (i), combinations of left and right loops (ii), of the left and right kinks (iii) or all these in combination (iv), giving rise to the axial tangling of filaments. From these micrographs we shall select and consider four different cases of tangling of vortex filaments. Fig. 2(i). shows vortex filaments each with a series of loops or a set of two-dimensional (2-D) solitons. These solitons have almost equidistant position (multisoliton system), representing a one-dimensional (1-D) soliton lattice. Fig. 3(i). shows two solitons (the left and the right loop) with corresponding wave vectors k_1^- and k_2^+, which travel in the same direction. If $v_2 > v_1$ the second soliton will collide with the first slower one from behind, and pass through it (Langer and Perline, 1994). Corresponding reconstruction is given in Fig. 3(ii). Fig. 4. shows two solitons (in the form of kinks) with the wave vectors k_1^+ and k_2^- (which travel in the same direction). In Fig. 4(i), the two different kinks can be formed by two (or more) alternating shocks from the left and right sides of the filament. Corresponding reconstruction is given in Fig. 4(ii). Fig. 5(a). shows a more complex filament organization of the "labyrinth type". Unfortunately, details of tangling are not quite clear even after numerical filtration. Approximate reconstruction of this tangling is given in stages (Fig. 5(b)). It starts with (i) two loops (basic configuration) on 2-D lattice, then (ii) continues with the formation of left and right loops on both sides of the filament, and (iii) eventually finishes with local reconnection. Topological transformation of tangled structure clearly shows two pairs of soliton loops of (+) and (−) wave vectors (iv).

In the following, we shall reconstruct some of these configurations with a filament (planar curve), which evolve in 2-D space according to integrable evolution equations (Nakayama et al., 1992). The curve is determined by the curvature, which is the solution of the modified Korteweg–de Vries (mKdV) equation. The one- and two-soliton solution for the curvature are obtained analytically by using the Hirota method.

3. Model

First, we assume that the motion of isolated vortex filament in an unbounded, incompressible and inviscid fluid is due to its own induction. The induced velocity is given by the Biot–Savart integral (Betchov, 1965). Localized induction equation (LIE) is an approximation for the Biot–Savart equation when the radius of curvature is much larger than the radius of the vortex core (Betchov, 1965). LIE describes asymptotic motion of the very thin isolated vortex filament with same curvature in perfect fluid (Betchov, 1965; Hasimoto, 1971; Hama and Nutan, 1961; Ricca, 1996):

$$\mathbf{r}_t = \kappa \mathbf{b}, \tag{1}$$

where $\mathbf{r}$ is the radius vector, κ is a curvature and $\mathbf{b}$ is the unit binormal vector. As long as the interaction between far distant portions along the filament is neglected, the approximation seems to be valid (Hasimoto, 1971).

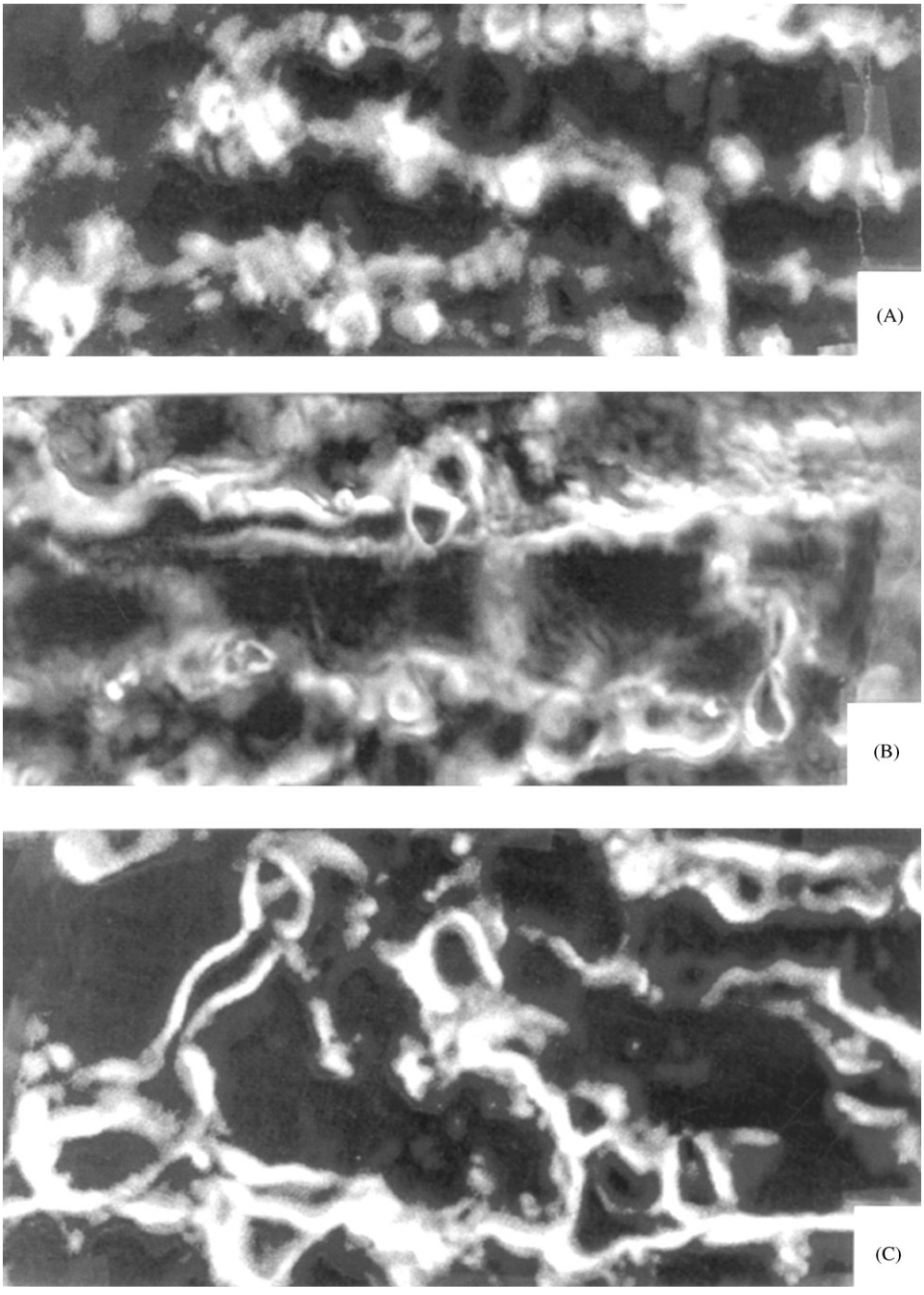

Fig. 1. Tangled structures of vortex filaments generated by XeCl excimer laser ($\tau = 16$ ns, $\lambda = 308$ nm) on Cr-coated steal surface. Three representative groups of axially tangled filaments follow the increasing order of topological complexity from (A) to (B) and to (C). $M \times$.

Second, we substitute vortex filament by the mathematical curve, the motion of which in space is described by the Frenet–Seret equations, i.e. the curve is completely described by the curvature and torsion. Hasimoto introduced the transformation (Hasimoto, 1971) $\psi = \kappa \exp\left(\mathrm{i} \int^s \tau \, ds\right)$, where τ is the torsion. In three-dimensional (3-D) space,

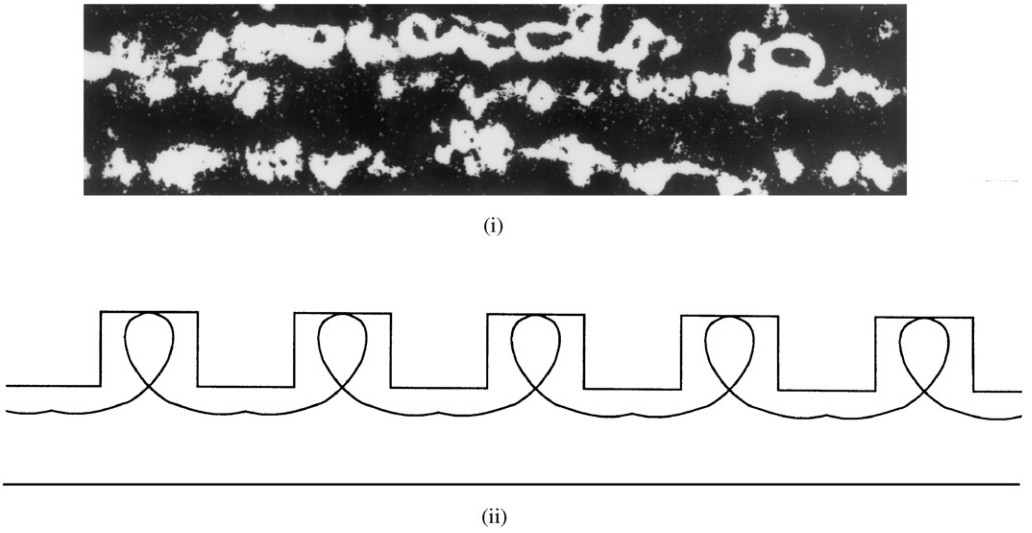

Fig. 2. (i) A series of 2-D solitons on filaments selected from Fig. 1A. (ii) Its reconstruction indicates the formation of 1-D soliton lattice. $M \sim 3800\times$.

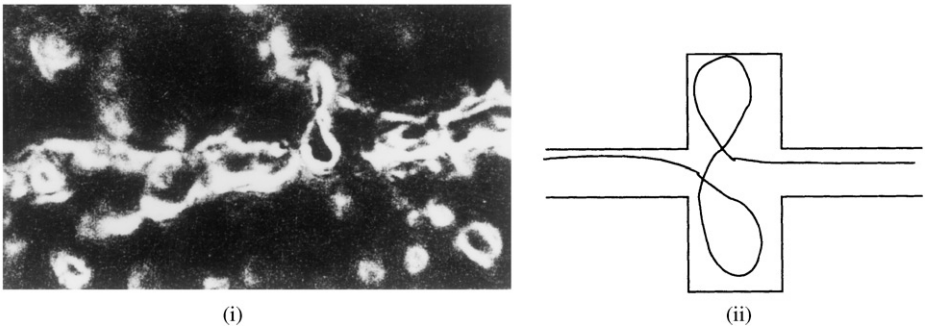

Fig. 3. (i) A segment of tangled filaments selected from Fig. 1B. (ii) Its reconstruction indicates the collision of two (loop) solitons of (+) and (−) wave vectors. $M \sim 3800\times$.

the Frenet–Seret equations and LIE can be combined with the Hasimoto transformation to yield a nonlinear Schrödinger equation:

$$\mathrm{i}\Psi_t + \Psi_{ss} + \tfrac{1}{2}|\Psi|^2\Psi = 0. \tag{2}$$

The curve is completely described by the Hasimoto transformation, Ψ. As in the case of the ideal fluid flow from which LIE is derived, it can be described as a Hamiltonian evolution equation which belong to an infinite hierarchy of commuting evolution equations, the so-called localized induction hierarchy (LIH) (Langer and Perline, 1994).

In two dimensions, we use planar filament (PF) equation as a evolution equation on planar curve (Nakayama et al., 1992; Langer and Perline, 1994):

$$\mathbf{r}_t = -\kappa'\mathbf{n} - \tfrac{1}{2}\kappa^2\mathbf{t}, \tag{3}$$

where $\mathbf{n}$ is the normal and $\mathbf{t}$ the tangent vector. The coordinates of the filament can be obtained by integrating the tangent vector. The PF equation is a member of LIH generated by using a recursive operator on LIE. The PF is an integrable system (Langer and Perline, 1994), which is related to the nonlinear evolution equation solved by the inverse scattering method (Nakayama et al., 1992). The Frenet–Seret equation in two dimensions.

$$\mathbf{t}' = \kappa\mathbf{n}, \qquad \mathbf{n}' = -\kappa\mathbf{t}, \tag{4}$$

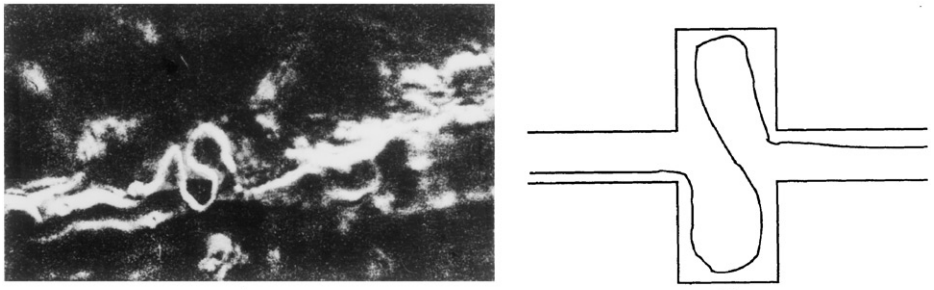

Fig. 4. (i) A segment of tangled filaments selected from Fig. 1B. (ii) Its reconstruction indicates the collision of two (kink) solitons of (+) and (−) wave vectors. $M \sim 3800\times$.

is the connection between the PF and mKdV equation for the curvature (as explained later). It was shown that most solutions do not represent the motion of the closed curve (Nakayama et al., 1992). It was shown in Goldstein and Petrich (1992) that PF equation (3) can be interpreted physically as localized induction equation for boundary of vortex patch for ideal fluid flow in two dimensions.

The filament obtained from LIE in 3-D space becomes a planar curve if torsion vanishes. Then, one soliton solution is equal up to some constant to the one soliton solution obtained from PF equation (compare solutions in Betchov (1965); Hasimoto, (1971); Lugomer and Maksimović, (1997)).

The filament length in this model is preserved, or in other words, the metric is constant. For simplicity, we use the normalized value of the metric:

$$g = \mathbf{r}' \cdot \mathbf{r}' = 1. \tag{5}$$

The compatibility condition requires that mixed partial derivatives of the radius vector must be equal (Nakayama et al., 1992): $\mathbf{r}_{st} = \mathbf{r}_{ts}$. The compatibility condition applied to Eq. (3) and first of the Frenet–Seret equations (4) yield the evolution equation for the tangent vector:

$$\mathbf{t}_t = -\left(\kappa'' + \tfrac{1}{2}\kappa^3\right)\mathbf{n}. \tag{6}$$

The compatibility condition of the tangent vector determines the integrable differential equation for the curvature. The curvature of the planar curve is a solution of the mKdV equation (Goldstein and Petrich, 1992; Nakayama et al., 1992):

$$\kappa_t + \kappa''' + \tfrac{3}{2}\kappa'\kappa^2 = 0. \tag{7}$$

We assume the same boundary condition $\kappa \to 0$ as $s \to \pm\infty$ as in Lugomer and Maksimović (1997) and Hasimoto (1971) and find the soliton solution. To obtain multisoliton solution we use the so-called "Hirota method" (Hirota, 1971; Hietarnita, 1997). The drawback of the Hirota's method is that it requires many algebra and calculus operations. The solution can be constructed with the aid of the symbolic programs based on the Hirota method (Hereman and Zhuang, 1992,1995; Hereman, 1992).

Using the transformation

$$\kappa = \frac{2}{\mathrm{i}}\left(\log\frac{F}{G}\right)_s, \tag{8}$$

where $F = f + \mathrm{i}g$ i $G = f - \mathrm{i}g$, one can transform the mKdV equation (7) into the bilinear form

$$P_1(D_x, D_t)(F \cdot G) = (D_t + D_x^3)(F \cdot G) = 0,$$

$$P_2(D_x, D_t)(F \cdot G) = D_x^2(F \cdot G) = 0. \tag{9}$$

Operators D_x, D_t are defined by the following relation:

$$D_x^m D_t^n (f \cdot g) = \left(\frac{\partial}{\partial x} - \frac{\partial}{\partial x'}\right)^m \left(\frac{\partial}{\partial t} - \frac{\partial}{\partial t'}\right)^n f(x,t)\, g(x',t')\Big|_{x'=x,t'=t}, \tag{10}$$

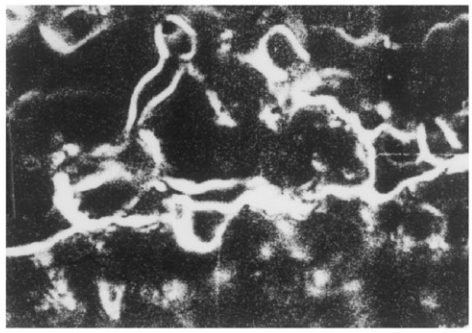

(a)

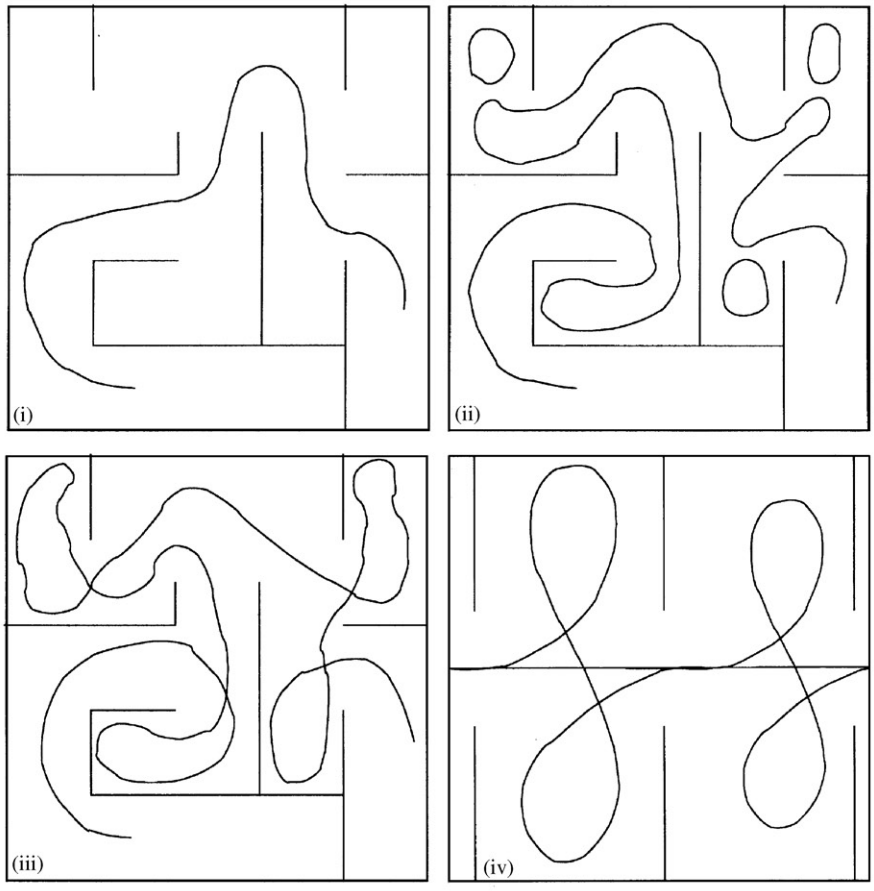

(b)

Fig. 5. (A) A segment of tangled filaments selected from Fig. 1C. (B) Its reconstruction indicates the collision of two-soliton trains of (+) and (−) wave vectors. Reconstruction given in segments from (i) to (iv), indicates the time evolution; see text. $M \sim 3800\times$.

where n, m are nonnegative integers (Hereman and Zhuang, 1992). P must be considered as a polynomial in its arguments. We look for a formal series solution for the unknown functions F_i, G_i $(i = 1, 2, 3, \ldots)$:

$$F = 1 + \varepsilon F_1 + \varepsilon^2 F_2 + \cdots,$$

$$G = 1 + \varepsilon G_1 + \varepsilon^2 G_2 + \cdots, \tag{11}$$

where $F_i = f_i + \mathrm{i}g_i$, $G_i = f_i - \mathrm{i}g_i$ and ε is a bookkeeping parameter (Hereman and Zhuang, 1992). Substituting Eq. (11) into bilinear form of the mKdV equation (9), and equating parts with same powers of ε, yields

$$\varepsilon^0 : B(1 \cdot 1) = 0, \tag{12}$$

$$\varepsilon^1 : B((f_1 \cdot 1 + 1 \cdot f_1) + \mathrm{i}(g_1 \cdot 1 - 1 \cdot g_1)) = 0, \tag{13}$$

$$\varepsilon^2 : B((f_2 + 1 \cdot f_2) + \mathrm{i}(g_2 \cdot 1 - 1 \cdot g_2) + (f_1 \cdot f_1 + g_1 \cdot g_1) + \mathrm{i}(g_1 \cdot f_1 - f_1 \cdot g_1)) = 0. \tag{14}$$

The operator B abbreviates the bilinear operator P_1 or P_2.

The tangent $\mathbf{t}$ and normal $\mathbf{n}$ vectors can be expressed in terms of the angle η, by using the following relations (Goldstein and Petrich, 1992):

$$\mathbf{t} = \mathrm{e}^{\mathrm{i}\eta} = (F/G)^2, \qquad \mathbf{n} = -\mathrm{i}\mathrm{e}^{\mathrm{i}\eta}, \tag{15}$$

where $\eta = \int \kappa ds = (2/\mathrm{i})\log(F/G)$.

Integral of the tangent vector is a radius vector. Using Eq. (15), one can calculate the analytical or numerical solution of the differential equation of the first order in symbolic programs such as `Mathematica`.

3.1. One-soliton solution

The simplest traveling wave solution of the mKdV equation is the one-soliton solution generated from

$$F = 1 + \mathrm{i}\mathrm{e}^{\theta}, \qquad G = 1 - \mathrm{i}\mathrm{e}^{\theta}, \tag{16}$$

where $\theta = ks - \omega t$, k and ω are constants. Eq. (12) is satisfied trivially, while Eq. (13) determines a dispersion law $\omega = k^3$. From Eq. (8) one can obtain the curvature of the loop

$$\kappa = \frac{2\,k\,\mathrm{e}^{\omega\,t+k\,s}}{\mathrm{e}^{2\,\omega\,t} + \mathrm{e}^{2\,k\,s}} = 2\,k\,\mathrm{sech}\theta,$$

which is the same result as in Lugomer and Maksimović (1997).

The radius vector of the curve is obtained by integration of the tangent vector (15). The coordinates are given as real and imaginary parts of the radius vector of the loop

$$x(s,t) = s - \frac{2}{k}\tanh\theta + C_1, \qquad y(s,t) = \frac{2}{k}\,\mathrm{sech}\,\theta + C_2, \tag{17}$$

where C_1 and C_2 are constants of integration. When the arc length s is equal to zero, we set the x and y coordinates to zero:

$$x(s,t) = s - \frac{2}{k}(\tanh\omega t + \tanh\theta),$$
$$y(s,t) = -\frac{2}{k}(\mathrm{sech}\,\omega t - \mathrm{sech}\,\theta). \tag{18}$$

The calculated solution for a fixed time is equal to the solution in Lugomer and Maksimović (1997) up to some constant. This solution represents the mirror image of the one calculated in Lugomer and Maksimović (1997), in which we used the so-called dual of the tangent vector (Goldstein and Petrich, 1992) $t^* = -\mathrm{i}\,\mathrm{e}^{\theta}$.

The soliton (loop) on vortex filament propagates from the left to the right with increasing time. The loop size of the soliton decreases as the value of the wave vector increases. A smaller loop travels faster than a larger loop. The path that the loop (maximum of the curve in the fixed time) wipes out has the form of the mirror image of the 2-D soliton curve. The mirror image is obtained by inserting a negative value of the wave vector, because $x(-k) = x(k), y(-k) = -y(k)$. The coordinates of the maximum were obtained from the coordinates by inserting time for which θ is equal to zero, $t = s/k^2$. The curve that was generated by the maximum is equal to the image curve at $t = 0$.

3.2. Two-soliton solution

The two-soliton solution is generated from

$$F = 1 + \mathrm{i}\mathrm{e}^{\theta_1} + \mathrm{i}\mathrm{e}^{\theta_2} - a_{1,2}\mathrm{e}^{\theta_1+\theta_2}, \tag{19}$$

$$G = 1 - \mathrm{i}\mathrm{e}^{\theta_1} - \mathrm{i}\mathrm{e}^{\theta_2} - a_{1,2}\mathrm{e}^{\theta_1+\theta_2}, \tag{20}$$

where $\theta_i = k_i s - \omega_i t$ $(i = 1, 2)$. As in the one-soliton solution, Eq. (13) determines a dispersion law $\omega_i = k_i^3$. The constant $a_{1,2} = (k_1 - k_2)^2/(k_1 + k_2)^2$ was calculated from Eq. (14). For the two-soliton solution of the mKdV equation, one finds

$$\kappa = \frac{-4\,\mathrm{i}\left(\dfrac{\mathrm{e}^{\theta_1+\theta_2}\left(\mathrm{i}\,\mathrm{e}^{\theta_1} + \mathrm{i}\,\mathrm{e}^{\theta_2}\right)(k_1-k_2)^2}{k_1+k_2} + \mathrm{i}\left(\mathrm{e}^{\theta_1}k_1 + \mathrm{e}^{\theta_2}k_2\right)\left(1 - \dfrac{\mathrm{e}^{\theta_1+\theta_2}(k_1-k_2)^2}{(k_1+k_2)^2}\right)\right)}{(\mathrm{e}^{\theta_1} + \mathrm{e}^{\theta_2})^2 + \left(1 - \dfrac{\mathrm{e}^{\theta_1+\theta_2}(k_1-k_2)^2}{(k_1+k_2)^2}\right)^2}. \tag{21}$$

Integrating the tangent vector (15) in the `Mathematica` program, we obtain the radius vector of the curve

$$\begin{aligned}\mathbf{r} = &-\frac{4\,\mathrm{i}\,\mathrm{e}^{k_2^3 t}k_1 + 4\,\mathrm{i}\,\mathrm{e}^{k_1^3 t}k_2 - 4\,\mathrm{e}^{k_1^3 t + k_2^3 t}(k_1+k_2)}{k_1 k_2\left(\left(\dfrac{k_1-k_2}{k_1+k_2}\right)^2 + \mathrm{i}\,\mathrm{e}^{k_1^3 t} + \mathrm{i}\,\mathrm{e}^{k_2^3 t} - \mathrm{e}k_1^3 t + k_2^3 t\right)}\\ &+\frac{k_1k_2s\left(\dfrac{k_1-k_2}{k_1+k_2}\right)^2 + \mathrm{i}k_2(4+k_1s)\mathrm{e}^{-\theta_1} + \mathrm{i}k_1(4+k_2s)\mathrm{e}^{-\theta_2} - \mathrm{e}^{-\theta_1-\theta_2}(4k_2 + k_1(4+k_2s))}{k_1k_2\left(\left(\dfrac{k_1-k_2}{k_1+k_2}\right)^2 + \mathrm{i}\mathrm{e}^{-\theta_1} - \mathrm{e}^{-\theta_1-\theta_2} + \mathrm{i}\mathrm{e}^{-\theta_2}\right)}\end{aligned} \tag{22}$$

Coordinates of the curve are real and imaginary parts of the previous equation. If the values of both wave vectors are equal to k, they can be expressed in somewhat simpler form

$$x = s + \frac{32}{3k}\left(\frac{1}{-5 + 3\tanh(k^3 t)} + \frac{1}{5 + 3\tanh(ks - k^3 t)}\right),$$

$$y = \frac{8}{k}\left(\frac{1}{-5\cosh(k^3 t) + 3\sinh(k^3 t)} + \frac{1}{5\cosh(ks - k^3 t) + 3\sinh(ks - k^3 t)}\right). \tag{23}$$

The solution is of the same form as the one-soliton solution; it is only delayed for approximately half a loop with respect to the one-soliton solution (not shown).

The two-soliton solution of mKdV equation (i.e. the curvature, κ) describes the interaction of two solitary waves. The distribution of intensity among both solitons can change during the collision (Radhakrishnan et al., 1997), but the total intensity remains constant. Larger solitary waves have greater speed, because the speed is proportional to the square of its amplitude (i.e. the phase velocity is equal to the square of its wave vector). The larger wave overtakes the smaller one and after fully nonlinear interaction the solitary waves re-emerge, retaining the same speed and form (Fordy, 1994). Only reminiscent of the interaction is the phase shift which represents the displacement of their centers. That is unlike from most dispersive equations which scatter solitary waves inelastically and dissipate their energy into radiation.

The ordinate of the soliton on vortex filament is inversely proportional to the wave vector, i.e. the larger the curvature the smaller and faster are the solitons. The collision of two solitons is elastic, since they emerge after collision with the unchanged speed and size. In Fig. 6, we show propagation of two solitons on the vortex filament for the wave vectors $k_1 = 3$ and $k_2 = 1$. Two solitons are initially separated and travel from the left to the right. After a while, smaller and faster soliton catches up the larger one near the origin of the coordinate system. One can observe (Fig. 6) that smaller soliton travels on the loop of the larger soliton. The smaller loop

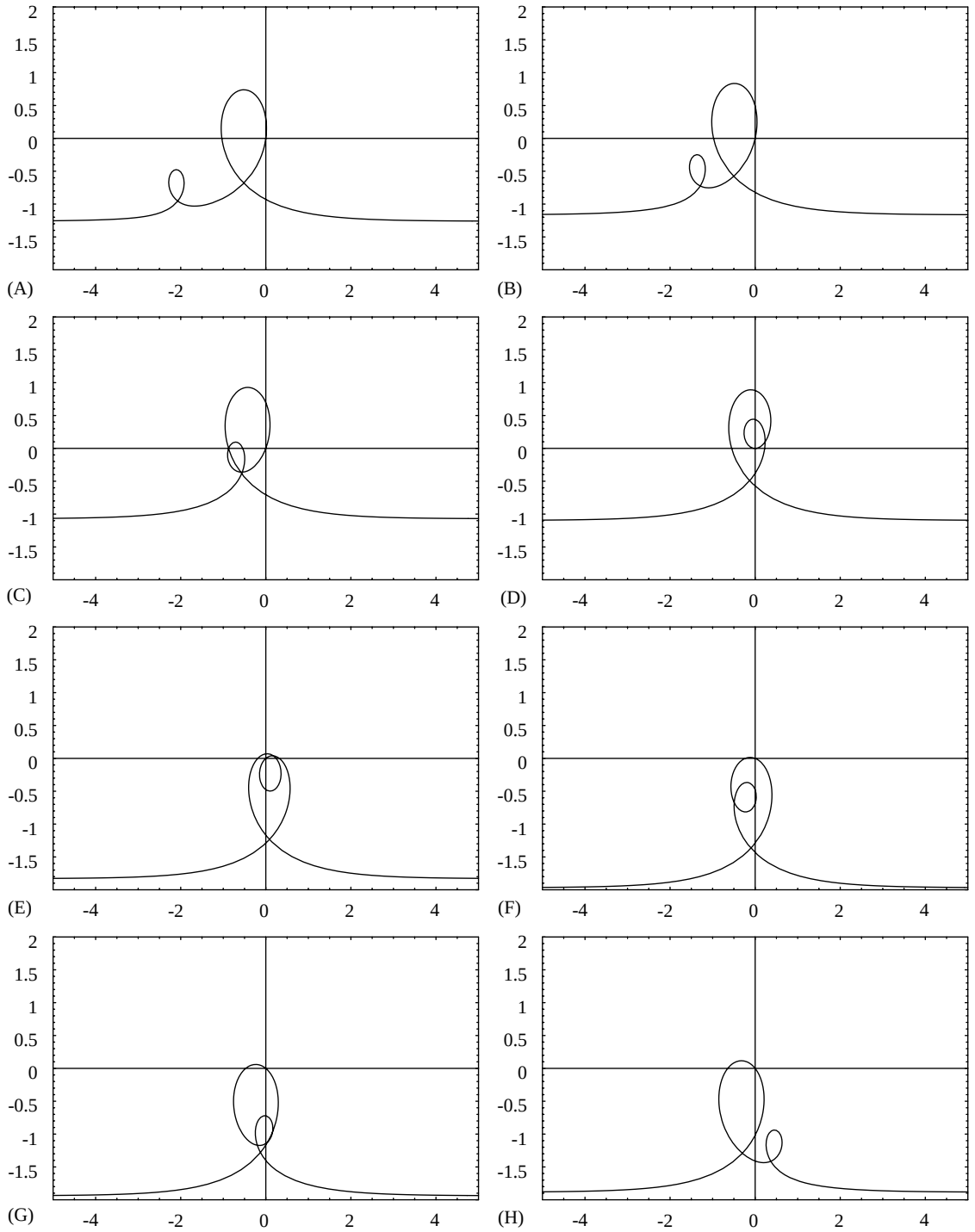

Fig. 6. Two-soliton solution for $k_1 = 3, k_2 = 1$: (A) $t = -0.35$; (B) $t = -0.25$; (C) $t = -0.15$; (D) $t = -0.05$; (E) $t = 0.05$; (F) $t = 0.15$; (G) $t = 0.25$; (H) $t = 0.35$.

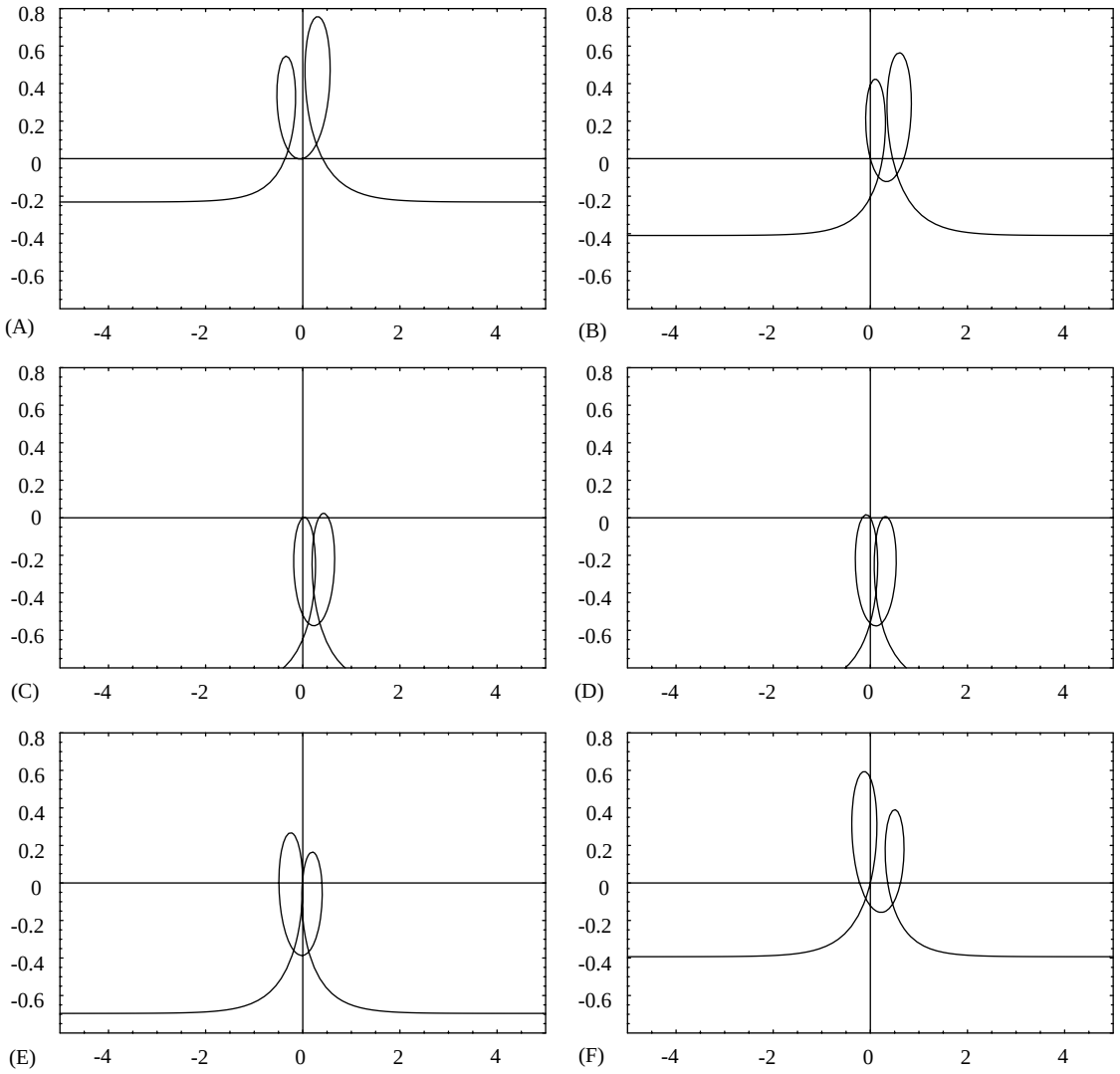

Fig. 7. Two-soliton solution for $k_1 = 3, k_2 = 2$: (A) $t = -0.1$; (B) $t = -0.02$; (C) $t = 0.06$; (D) $t = 0.08$; (E) $t = 0.14$; (F) $t = 0.22$.

inside the larger can be distinguished since there is significant difference in the intensity of two solitons. The contour of the curvature shows the shift of the trajectory only for the soliton with a larger wave vector, i.e. for the smaller loop.

If the values of two wave vectors are much closer, for example $k_1 = 2$ and $k_2 = 3$, the smaller loop travels to the right faster than the larger soliton (see Fig. 7). Since the difference in their intensity is not as great as in the previous case, the smaller soliton does not travel along the loop of the larger one. When smaller and faster soliton catches up the larger one (near the origin of the coordinate system), there is a soliton exchange. The two components redistribute from the larger to the smaller one, while they are moving together in a loop around the origin of the coordinates. After the loop is completed, the smaller one is on the right side and continues to go away with the same speed as before the collision.

If one of the wave vectors is negative, then one of the loops is inverted with respect to the abscissa axis. Exchanging the signs of two wave vectors we can flip two loops around the abscissa. In Figs. 8 and 9, we show the propagation of two solitons on the vortex filament for two different sets of the wave vector values. The situation is the same as in the first case where the wave vectors are different (enough), so that one can distinguish between two solitons when they overlap. The smaller soliton again travels on the loop of the larger one.

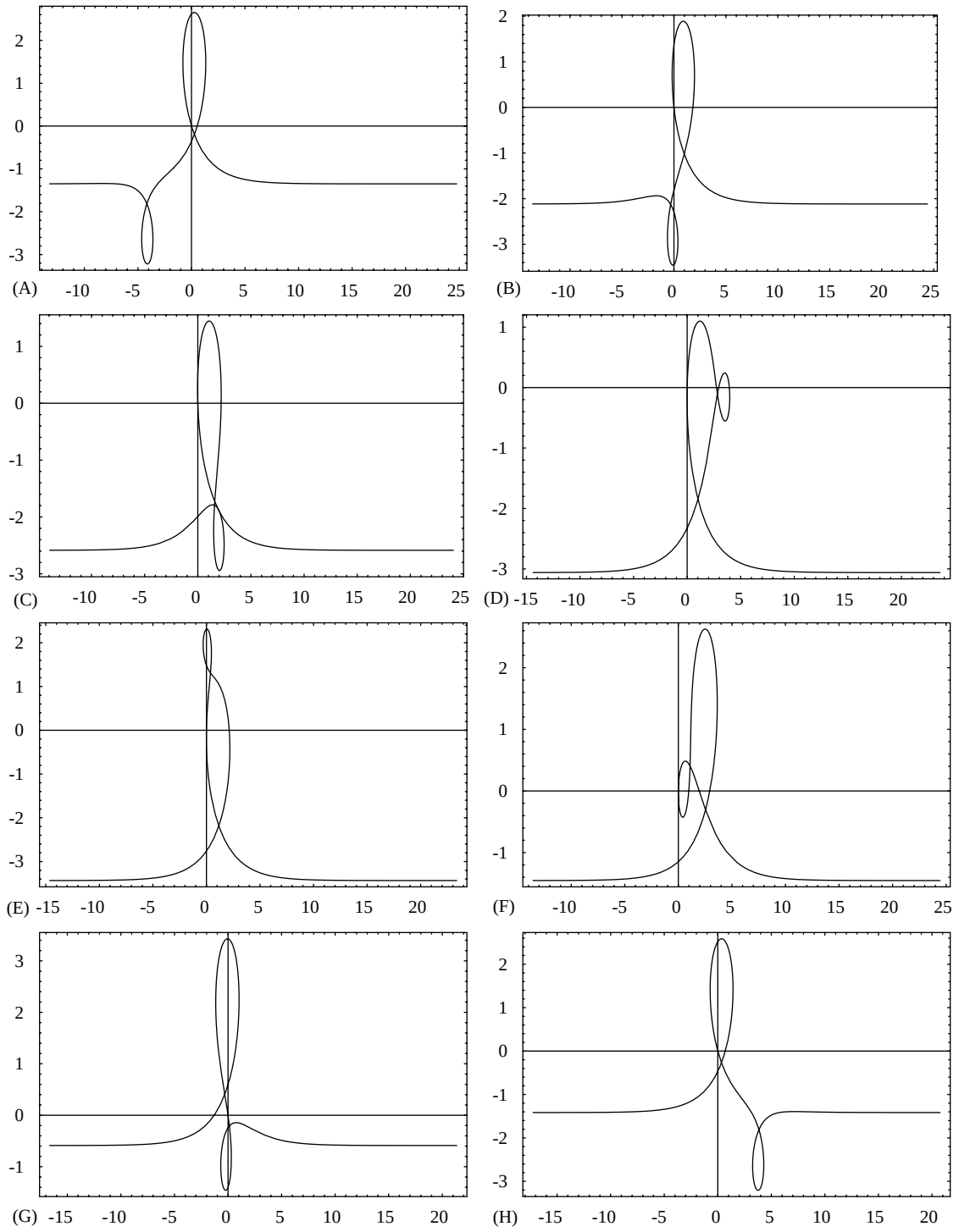

Fig. 8. Two-soliton solution for $k_1 = \frac{1}{2}, k_2 = -1$: (A) $t = -14$; (B) $t = -10$; (C) $t = -8$; (D) $t = -6$; (E) $t = -4$; (F) $t = -2$; (G) $t = 0$; (H) $t = 4$.

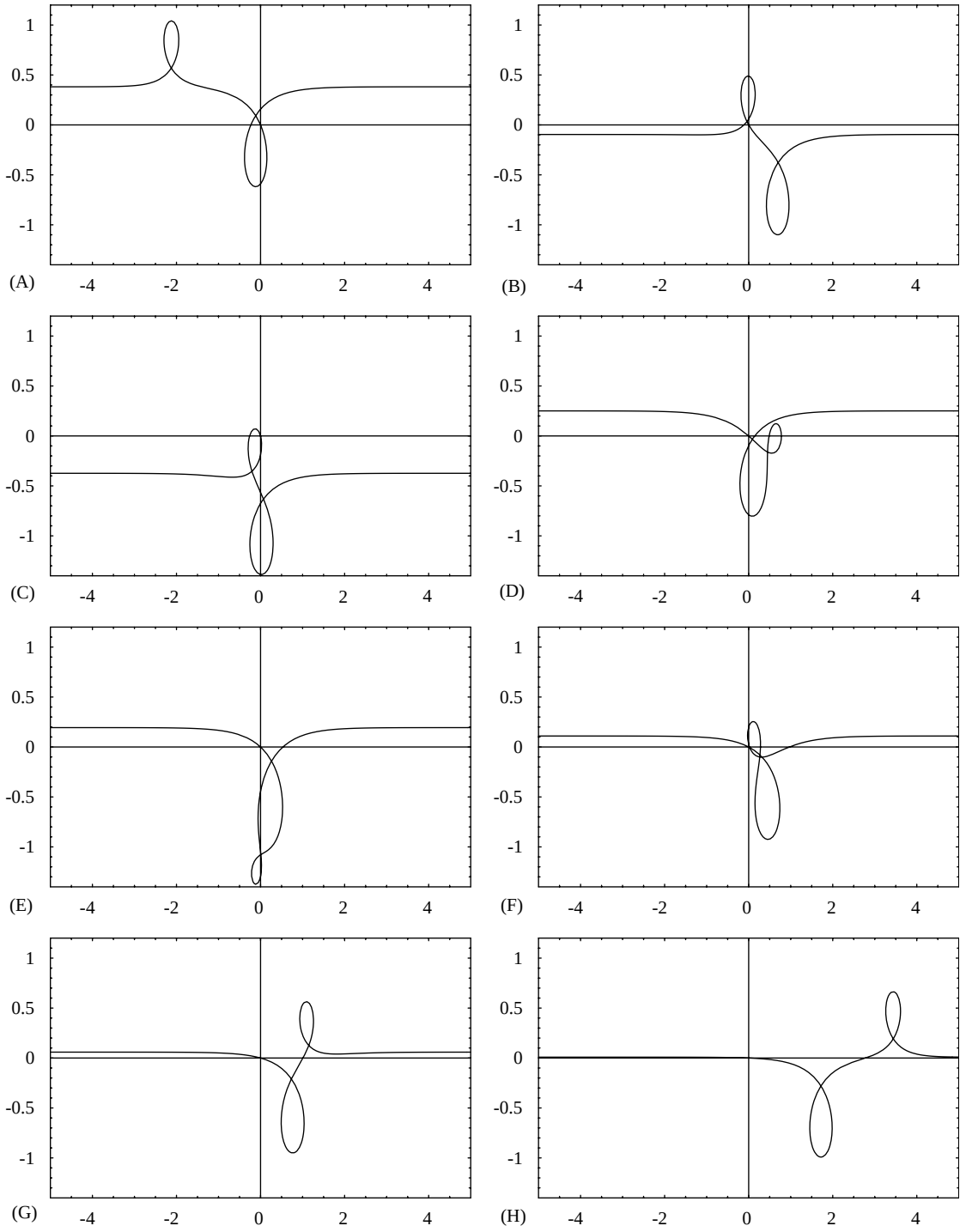

Fig. 9. Two-soliton solution for $k_1 = 3, k_2 = -2$: (A) $t = -0.2$; (B) $t = 0.12$; (C) $t = 0.2$; (D) $t = 0.28$; (E) $t = 0.36$; (F) $t = 0.44$; (G) $t = 0.52$; (H) $t = 0.76$.

4. Conclusion

The experimental study of tangling of vortex filaments in laser–matter interactions and theoretical study, based on the analytical solutions of the filament dynamics, have shown that axial tangling of filaments occurs by generation of multisolitons of various types (loops, kinks, etc.) of positive and negative wave vector in sequences. Such a situation caused by the shock waves associated with a series of laser pulses, leads to various kinds of tangling with different levels of topological complexity. Topological transformation of tangled segments reveal that their "basic elements" are common to (almost) all observed tanglings. Approximated by a combination of 2-D solitons which collide from behind, they have been reconstructed by the analytical solution for the radius vector (Eq. (22) of the planar curve. The curvature of the curve is found by the Hirota method. Although the exact agreement between observed (real) tangled structures and those obtained mathematically cannot be expected because of complexity of the real situation in the experiment, the similarity is really impressive. These studies indicate that 2-D solitons with combined wave vectors $k_1^+, k_2^-, \ldots, k_n^{(+),(-)}, \ldots$, which travel in the same direction with different speed will collide and cause the tangling of a filament. The most elementary case of tangling represents a series of 2-D solitons (loops), which move with (approximately) the same velocity in the same direction (forming a 1-D soliton lattice). Since there is no collision from behind, they travel as a soliton train.

A complex case occurs when two solitons of the *same polarity* of the wave vector (either + or −) collide from behind. A more complex case occurs when two solitons of *different polarity* collide from behind. Finally, the most complex case observed occurs when a series of solitons with alternating polarity collide, leading to the "labyrinth" type of tangling. It follows that labyrinth tangling is a consequence of random shock waves (which generate the alternating polarity of solitons) and, in addition, of random distribution of velocity of the solitons on filaments. The above classification of the observed cases elucidates the origin of hierarchy in topological complexity of the axial tangling filaments in LMI.

References

Betchov, R., 1965. On the curvature and torsion of an isolated vortex filament. Journal of Fluid Mechanics 22, 471–479.

Crabtree, G.W., Nelson, D.R., 1997. Vortex physics in high-temperature superconductors. Physics Today 50, 38–45.

Fordy, A.P., 1994. A historical introduction to solitons and Bäcklund transformations. In: Fordy, A.P., Wood, J.C. (Eds.), Harmonic Maps and Integrable Systems. Aspects of Mathematics. Vieweg, Braunschweig, Wiesbaden, pp. 7–28.

Geller, M.J., Huchra, J.P., 1989. Mapping the Universe Science 246, 897–903.

Goldstein, R.E., Petrich, D.M., 1992. Solitons, Euler's equation, and vortex patch dynamics. Physical Review Letters 69, 555–558.

Hama, F.R., Nutan, J., 1961. Self-induced velocity on a curved vortex. Physics of Fluids 4, 28–32.

Hasimoto, H., 1971. A soliton on a vortex filament. Journal of Fluid Mechanics 51, 447–485.

Hereman, W., 1992. Symbolic Software for the study of nonlinear partial differential equations. In: G. Richter (Ed.), Proceedings of the IMACS PDE7 International Conference, New Brunswick, NJ. e-print, ftp://ftp.mines.edu/pub/papers/math_cs_dept/software/pdeimacs.tex.

Hereman, W., Zhuang, W., 1992. Symbolic computation of solitons with Macsyma. In: W.F. Ames, P.J. van der Houwen (Eds.), Proceedings of the 13th IMACS World Congress Dublin, pp. 287–296.

Hereman, W., Zhuang, W., 1995. Symbolic software for soliton theory. Acta Applicandae Mathematicae 39, 361–378.

Hietarnita, J., 1997. Introduction to the Hirota bilinear method. In: Lectures on the Integrability of Nonlinear Systems, Springer Lecture Notes in Physics, Vol. 495, Springer, Berlin, e-print, http://xyz.lanl.gov/e-print/solv-int/9708006.

Hirota, R., 1971. Exact solution of the Korteweg–de Vries equation for multiple collisions of solitons. Physical Review Letters 27, 1192–1194.

Jeanloz, R., Romanowicz, B., 1997. Geophysical dynamics at the center of the earth. Physics Today 50, 22–27.

Kolton, A.B., Dominguez, D., 1999. Hall noise and transverse freezing in driven vortex lattices. Physical Review Letters 83, 3061–3064.

Langer, J., Perline, R., 1994. The planar filament equation. Fields Institute Proceedings, Mechanics Days, June. e-print, http://xyz.lanl.gov/e-print/solv-int/9403001.

Lugomer, S., Maksimović, A., 1997. Solitons on vortex filaments generated by ns laser pulse on metal surface. Journal of Applied Physics 82, 1374–1383.

Lugomer, S., 1999. Braids of vortex filaments generated by laser on metal surface. Physics Letters A 259, 479–487.

Nakayama, K., Segur, H., Wadati, M., 1992. Integrability and the motion of curves. Physical Review Letters 69, 2603–2606.

Norman, M.L., 1996. Probing cosmic mysteries by supercomputer. Physics Today 49, 42–48.

Radhakrishnan, R., Lakshmanan, M., Hietarinta, J., 1997. Inelastic collision and switching of coupled bright solitons in optical fibers. Physical Review A 56, 2213–2216 e-print, http://xyz.lanl.gov/e-print/solv-int/9703008.

Ricca, R.L., 1996. The contributions of Da Rios and Levi-Civita to asymptotic potential theory and vortex filament dynamics. Fluid Dynamics Research 18, 245–268.

Ricca, R.L., Berger, M.A., 1996. Topological ideas and fluid mechanics. Physics Today 49, 28–34.

Schönenberger, A., Larkin, A., Heeb, E., Geshkenbein, V., Blatter, G., 1996. Strong pinning and plastic deformations of the vortex lattice. Physical Review Letters 77, 4636–4639.

Schwartz, K.W., 1998. Three-dimensional vortex dynamics in superfluid 4He: Homogeneous superfluid turbulence. Physical Review B 38, 2398–2408.

Schwartz, K.W., 1985. Three-dimensional vortex dynamics in superfluid 4He: Line-line and line-boundary interactions. Physical Review B 31, 5782–5794.